



Hybrid laser metal deposition of a Fe–Cr–Mo–V–Mn tool steel for hot stamping applications

Tobia Romano¹ · Marawan Abdelwahed^{1,2} · Sven Bengtsson³ · Francesco Bruzzo⁴ · Riccardo Casati¹ · Hans Gedda⁵ · Elena López⁴ · Petter Ulfberg⁵ · Christoph Wilsnack⁴ · Maurizio Vedani¹

Received: 15 March 2022 / Accepted: 7 January 2023
© The Author(s) 2023

Abstract

In this investigation, a novel Fe–Cr–Mo–V–Mn hot work tool steel powder was specifically developed for laser-based additive manufacturing, targeting the possibility to create conformal cooling channels in hot stamping tools for improved cooling efficiency during the forming of steel sheets for the automotive industry. Specimens of the proposed tool steel were printed via laser metal deposition and characterized to demonstrate its compatibility with hot work tool steels that are commonly used in the tooling industry. The applicability of the developed material was proved by fabricating cooling channels in a simple geometry demonstrator using a hybrid process combining milling and laser metal deposition. Finally, a hybrid-manufactured hot stamping tool segment was tested in a pilot plant to evaluate the effect of the investigated material on the cooling performance when compared to a conventional tool machined from H13 hot work tool steel. The results showed that the Fe–Cr–Mo–V–Mn tool steel features thermophysical properties similar to the most popular H13 steel and it can be efficiently used to produce tools containing conformal cooling channels by hybrid laser metal deposition, without the need of intermediate structures to improve the compatibility between the substrate and the deposited volumes.

Keywords Hybrid additive manufacturing · Laser metal deposition · Hot stamping · Conformal cooling channels · Tool steel · Thermal diffusivity

1 Introduction

Lightweight is one of the main trends within body-in-white design, as it translates into a combined reduction of raw material use and fuel consumption [1], therefore highlighting the environmental benefits during both the manufacturing and use of vehicles [2, 3]. Hot stamping is a widespread forming technology in the automotive industry, which enables the manufacturing of lightweight automotive

components, such as B-Pillars and door impact beams, with high strength and crash performance [4, 5], thus ensuring both fuel saving and passenger safety. Hot stamping involves heating of the steel blank above the austenitization temperature, followed by simultaneous forming and quenching in a closed tool [4]. Under high cooling rates (of the order of several tens of °C s⁻¹ [1]), the steel microstructure transforms into martensite, leading to high hardness and strength of the formed part. The rapid cooling of the blank and tool is achieved by a network of internal channels where a cooling fluid, typically water, flows. In conventional manufacturing processes, straight cooling channels are simply machined in the tools by drilling [4]. However, this design shows some limitations. Since straight cooling channels cannot always match the surface curvature of the tool, they cannot guarantee a uniform heat extraction from the hot blank, which may cause warpage due to non-uniform stress states in the formed part [6] and incomplete martensitic transformation in regions where the local cooling rate is insufficient, thus resulting in inadequate mechanical properties [4]. In addition, a lower cooling efficiency increases the process cycle

✉ Tobia Romano
tobia.romano@polimi.it

¹ Department of Mechanical Engineering, Politecnico di Milano, 34 La Masa, 20156 Milan, Italy

² Department of Design and Production Engineering, Faculty of Engineering, Ain Shams University, Cairo, Egypt

³ Höganas AB, Höganas, Sweden

⁴ Fraunhofer Institute for Material and Beam Technology IWS Dresden, Dresden, Germany

⁵ Gestamp Hardtech SA, Luleå, Sweden

time, thus affecting the productivity, and reduces the lifetime of tools subjected to higher in-service temperatures.

The use of conformal cooling channels has been proposed as an approach to improve the cooling efficiency in hot stamping tools [5]. However, topologically optimized cooling channels usually feature complex curved shapes that are difficult or even impossible to be manufactured using conventional technologies [7]. Groove milling has been proposed as an alternative to straight drilling for the production of molds and tools containing conformal cooling channels [8]. Each tool face is designed in two halves. Grooves are milled on one face according to the expected surface curvature of the tool, while the other face is used to cover them and obtain a network of channels [8]. Despite the ease of fabrication, several gaskets and O-rings are required in bolted joints or, alternatively, even more complex bonding techniques may be needed to achieve a good seal and avoid coolant leakage [7, 9].

Metal additive manufacturing (AM) raised the possibility to print molds, tools, and dies already containing conformal cooling channels without any machining time and material waste [10–14]. The design freedom offered by AM could be exploited even further to fabricate the volumes containing the conformal cooling channels and forming surface of the tool, while the main body could still be manufactured using subtractive methods to limit the overall production time and costs. Muvunzi et al. [1, 15] successfully fabricated hot stamping tools with conformal cooling channels using a hybrid technology which combined machining and Laser Powder Bed Fusion (LPBF). However, it was challenging to achieve a perfect alignment of the surface in the LPBF machine to correctly start the printing process. Designing a common heat treatment suitable for both the machined and the deposited sections, made of two dissimilar materials, was also a source of compromise. One inherent limitation of LPBF is the strict requirements of a flat surface for a successful deposition of the powder bed [16], which may not always be possible when dealing with complex tool geometries. Liu et al. [17] also showed that the relatively high roughness of the inner surface of cooling channels manufactured through LPBF hinders the flow of the cooling fluid, leading to a lower performance compared to a system of drilled channels with the same geometry.

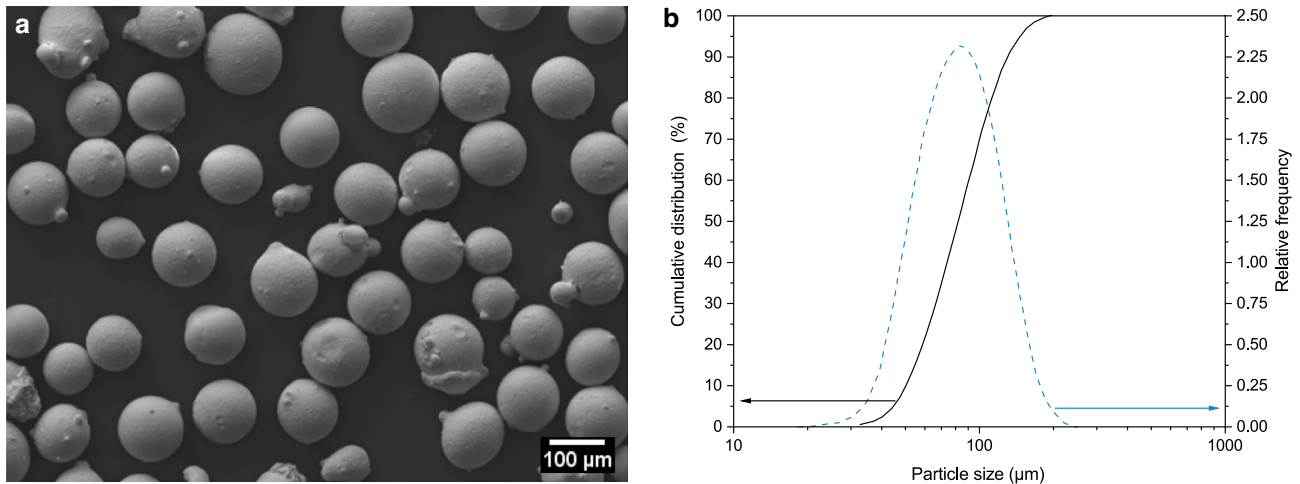
Direct deposition AM technologies such as Laser Metal Deposition (LMD) are capable of free-form manufacturing with almost no geometrical restrictions and are particularly suited for adding features to existing parts without the need for a flat base surface, since the feedstock material is melted immediately as it is deposited during the process [18].

Compared to LPBF, LMD can fabricate larger parts, as in principle it does not require an enclosed work chamber, and can be more easily combined with machining tools to mechanically finish the inner surface of the channels as they are built up layer by layer [7], resulting in a better surface quality. In addition, the substrate can be conveniently oriented during the process to always deposit the material in the vertical direction, avoiding the issues related to the fabrication of overhanging structures. Cortina et al. [19] fabricated a hot stamping die with conformal cooling channels using a hybrid process combining milling and LMD. First, they machined the bottom half of a duct on the surface of the tool base, made of CR7V-L hot work tool steel, ending with a 45° V-notch to facilitate the following LMD operation. Then, they additively created the upper vault of the channel by depositing an initial 316L stainless steel intermediate layer, followed by a H13 hot work tool steel cover. The 316L buffer layer allowed avoiding the formation of cracks that would have otherwise appeared at the interface between the two hot work tool steels. A hybrid manufacturing strategy was also adopted by Hong et al. [20] to fabricate a hot stamping tool with conformal cooling channels. They machined hemispherical channels on a base plate made of S45C structural steel and closed them with HTCS-150 hot work tool steel hemispherical coupons. Finally, a HTCS-150 surface layer was deposited by LMD. In both case studies, an intermediate structure was needed to improve the compatibility between the machined and the additively manufactured sections of the tool, which increased the complexity of the overall manufacturing process.

Despite the promising results in the fabrication of hot stamping tools with conformal cooling channels, LMD is not yet fully established in industrial applications. One of the main reasons is the limited availability of materials with suitable mechanical and thermal properties combined with good LMD processability [21]. The present study investigates a novel Fe–Cr–Mo–V–Mn hot work tool steel grade especially tailored for AM and its use in combination with conventional hot work tool steels. The target application was the fabrication of hot stamping tools with conformal cooling channels by a hybrid technology integrating conventional machining and LMD. First, the processing parameters were optimized for the LMD of the Fe–Cr–Mo–V–Mn alloy and the thermo-physical properties of the printed material were characterized to demonstrate its compatibility with steel grades used in tool and die manufacturing. Then, the proposed alloy was used to integrate cooling channels on a machined H13 hot work tool steel body via LMD without any interlayer material. Finally, the performance of a hybrid-manufactured hot stamping tool segment was assessed by testing it in a pilot plant.

Table 1 Chemical composition (in weight %) of Fe–Cr–Mo–V–Mn and H13 hot work tool steel grades

Material	Cr	Mo	V	Si	C	Mn	P	S	Fe
Fe–Cr–Mo–V–Mn	6.03	2.06	1.01	0.77	0.36	0.20	–	–	Bal.
H13 (ASTM A681 [22])	4.75–5.5	1.1–1.75	0.8–1.2	0.8–1.25	0.32–0.45	0.2–0.6	0.03	0.03	Bal.

**Fig. 1** a SEM micrograph and b particle size distribution of the Fe–Cr–Mo–V–Mn powder**Table 2** Fe–Cr–Mo–V–Mn powder characteristics

Apparent density	Hall flaw rate	Particle size		
		D ₁₀	D ₅₀	D ₉₀
4.42 g cm ⁻³	15.0 s ⁻¹	50 μm	82 μm	126 μm

2 Materials and methods

2.1 Feedstock powder for LMD

A gas atomized Fe–Cr–Mo–V–Mn tool steel powder was developed and supplied by Höganäs AB. The chemical composition of the investigated powder is provided in Table 1 and compared with ASTM standard H13 hot work tool steel [22]. The developed powder contains around 15% and 30% increase in chromium and molybdenum contents, respectively, compared to H13 alloy. Figure 1 displays the spherical morphology of the powder particles and the size distribution measured with a Sympatec particle size analyzer. Apparent density, Hall flaw rate, and particle size characteristics of the powder are reported in Table 2.

2.2 Development of LMD process parameters and post-process heat treatment

The LMD process optimization for the proposed steel was carried out in a DMG Mori Lasertec 65 DED Hybrid system

using a 316L stainless steel substrate. A fiber coupled diode laser source from Laserline having a maximum power of 4 kW and a spot size of 1.6 mm was used during the manufacturing process. The powder was delivered from an external feeder (type GTV PF 2/2) to a COAX14V5 nozzle having a powder spot size of 1.6 mm at a distance of 12.5 mm from the substrate. The powder cone was scanned with a LIsec system from Fraunhofer IWS, and the powder spot size was measured as the smallest area through which 86% of the blown powder passes.

Laser power, deposition speed, and powder feed rate were first adjusted to deposit stable single tracks. Then, the optimization of the geometrical parameters (hatching distance and layer thickness) was carried out through the deposition of small volumes, as shown in Fig. 2. The optimal process parameters, leading to crack-free deposits with a limited fraction of residual porosity, are listed in Table 3. Each layer was created employing a bidirectional deposition strategy with laser off between tracks. Also, the scanning direction was rotated by 90° after each layer. This strategy, involving the deposition of alternating longitudinal and transversal tracks, prevents the generation of directional residual stress in the material, which promotes the formation of cracks in LMD deposits [19]. No holding time was used after the deposition of each layer.

A group of printed specimens was subjected to a multi-stage heat treatment, as shown in the diagram of Fig. 3. The treatment consisted of a first annealing step at 850 °C for

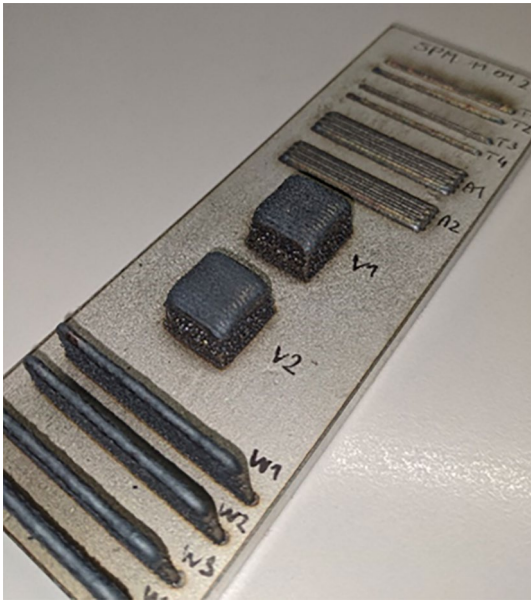


Fig. 2 Test runs of single tracks, single layers, cube volumes, and thin walls for the optimization of the geometrical process parameters

Table 3 Set of parameters resulting from LMD process optimization

Parameter	Value
Laser power	825 W
Deposition speed	750 mm min ⁻¹
Powder feed rate	8.3 g min ⁻¹
Track width	1.45 mm
Tracks overlap	35%
Layer thickness	0.9 mm
Shielding gas flow rate	7 l min ⁻¹
Carrier gas flow rate	10 l min ⁻¹

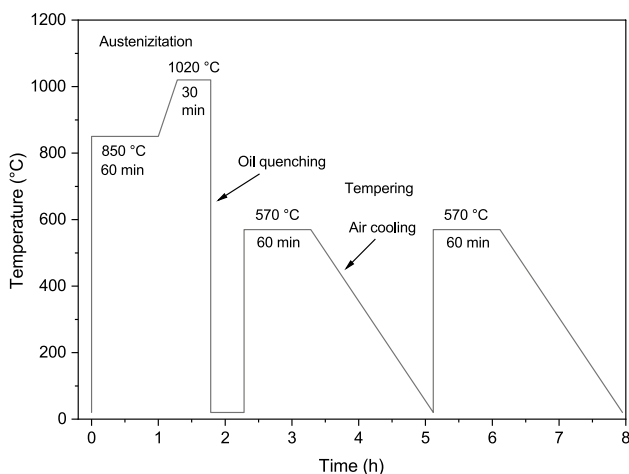


Fig. 3 Heat treatment schedule applied on LMD-processed specimens

Table 4 Phase transformation temperatures (in °C) of Fe–Cr–Mo–V–Mn and H13 hot work tool steel predicted with ThermoCalc AB software

Material	Ac ₁	Ac ₃	Ms	Mf
Fe–Cr–Mo–V–Mn	858	886	255	180
H13 (ASTM A681 [22])	850	878	249	173

60 min, followed by a second annealing step at 1020 °C for 30 min. Later, the specimens were quenched in oil and subjected to double tempering treatment at 570 °C for 60 min with air cooling between cycles. This thermal profile was defined based on the recommended heat treatment practices for H13 hot work tool steel [23, 24] and considering the phase transformation temperatures predicted by thermodynamic simulations performed with ThermoCalc AB software relying on an equilibrium TCFE 9.2 database for the investigated material and for a H13 steel with the standard chemical composition reported in Table 1. As reported in Table 4, slightly higher transformation temperatures were obtained for the Fe–Cr–Mo–V–Mn alloy compared to H13 steel. This is attributed to the higher chromium and molybdenum content of the proposed alloy, which broaden the stability field of ferrite [25], thus increasing the austenitic and martensitic transformation temperatures.

2.3 Characterization of LMD specimens

Figure 4a shows a picture of one cubic specimen built by LMD. A mismatch can be seen between the contour and the infill region of the samples. This is because process parameters were adjusted only for the inner region since a contour strategy was not employed to manufacture the demonstrator. The density of as-built parts was determined by the immersion method based on Archimedes' buoyancy principle, using a Mettler Toledo scale and employing distilled water at 20 °C as a reference liquid for the measurement. The values reported below are the average of seven measurements. The microstructure of as-built and heat-treated specimens was observed by a Nikon Eclipse LV150NL optical microscope and a Zeiss Sigma 500 field-emission scanning electron microscope (FE-SEM), exposing sections on planes parallel to the lateral surface (YZ) and perpendicular to the building direction (Z). After sectioning, the specimens were prepared according to standard metallographic procedures and polished up to 1 μm diamond suspension. The as-built specimens were etched by a Nital 2% solution (2 vol% nitric acid and 98 vol% ethanol) for 270 s to reveal the microstructure. The immersion time was reduced to 120 s for heat-treated specimens. Vickers hardness of the LMD processed material was measured along the building direction with 1 mm steps, starting from the top of the deposit

Fig. 4 View of the LMD specimens used for **a** microstructure analysis, **b** dilatometry, and thermal diffusivity tests

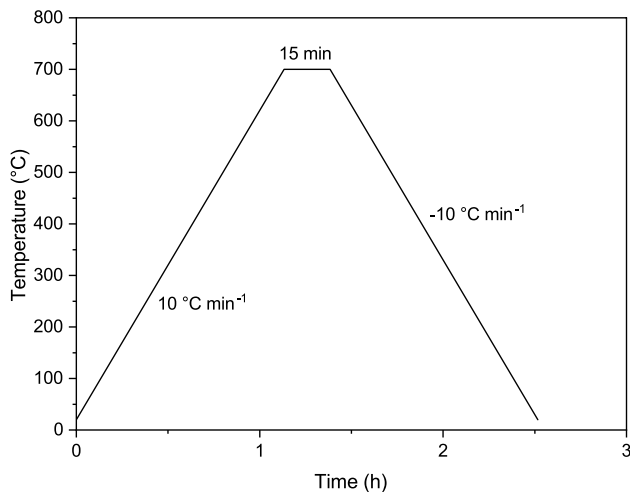
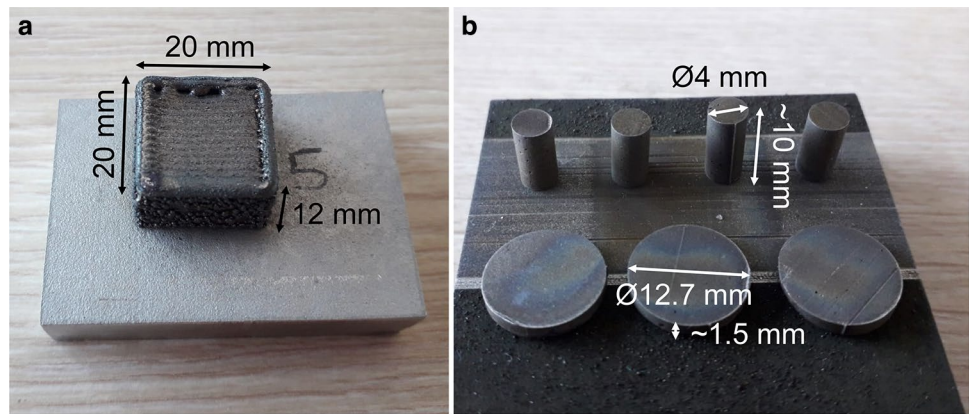


Fig. 5 Heating profile used in dilatation experiments

down to the 316L stainless steel substrate, by employing a HP-Mikromat 1 hardness tester using the testing routine for $HV_{0.3}$ (ISO 6507-1:2018).

Specimens for dilatometry tests and laser flash analysis (LFA) were extracted from both as-built and heat-treated samples by electrical discharge machining (EDM), as depicted in Fig. 4b. The dilatometry experiments were performed in argon atmosphere (1.2 bar pressure; 2 nl h^{-1} flow rate) by applying the thermal profile given in Fig. 5, using a Linseis L75 vertical dilatometer. LFA was performed with a Linseis LFA 1000 equipment in a dynamic vacuum environment under $\sim 1.2 \cdot 10^{-2}$ mbar, employing a 350 V laser voltage with 1 ms pulse duration and a $5 \text{ }^\circ\text{C min}^{-1}$ nominal heating rate. Both faces of the LFA specimens were grinded and polished up to $6 \text{ }\mu\text{m}$ diamond suspension. Then, a thin graphite layer was sprayed on both faces to increase the absorption of laser energy, which is essential for metallic materials with relatively high reflectivity. Thermal diffusivity values were collected from room temperature to $500 \text{ }^\circ\text{C}$ with increments of $25 \text{ }^\circ\text{C}$, performing three measurements for each step with an allowance of $\pm 7 \text{ }^\circ\text{C}$. ASTM E228-17 and

E1461-13 standards were used as a reference for the experimental procedures.

2.4 Hybrid LMD cooling channel feasibility

A simplified demonstrator with planar geometry was first manufactured to assess the processability of conformal cooling channels in hot stamping tools using the investigated Fe–Cr–Mo–V–Mn alloy and the developed LMD process parameters. The main body of the demonstrator, made of H13 hot work tool steel, was first machined producing grooves for the lower half of the cooling channels (Fig. 6a) and 45° V-notches in the upper part to facilitate the following material deposition by LMD. Then, 5-axis LMD was performed to create the upper vaults of the ducts using the approach shown in Fig. 6b. During the process, the substrate was continuously tilted by $\pm 40^\circ$ to grow the deposit along the vertical direction (Fig. 6c) by cladding longitudinal tracks alternately on the right and left side of the V-notch. Finally, additional layers were deposited to the whole surface to achieve the desired profile. The use of the Fe–Cr–Mo–V–Mn powder allowed fabricating bimetallic cooling channels by direct deposition on the H13 hot work tool steel substrate without the need of interposing any intermediate buffer layer.

2.5 Hot stamping tool prototyping

To assess the actual performance under real use of the proposed steel, a hot stamping die segment containing cooling channels was fabricated according to a procedure similar to that described above and tested in a pilot plant provided by Gestamp Hardtech SA.

Large stamping tools are normally built by joining multiple segments (Fig. 7), which are individually machined before their assembly [5]. Therefore, a single tool segment (Fig. 8c) was designed for the hot stamping of the sheet profile shown in Fig. 8b. One side of the segment was manufactured by conventional machining only, starting from a

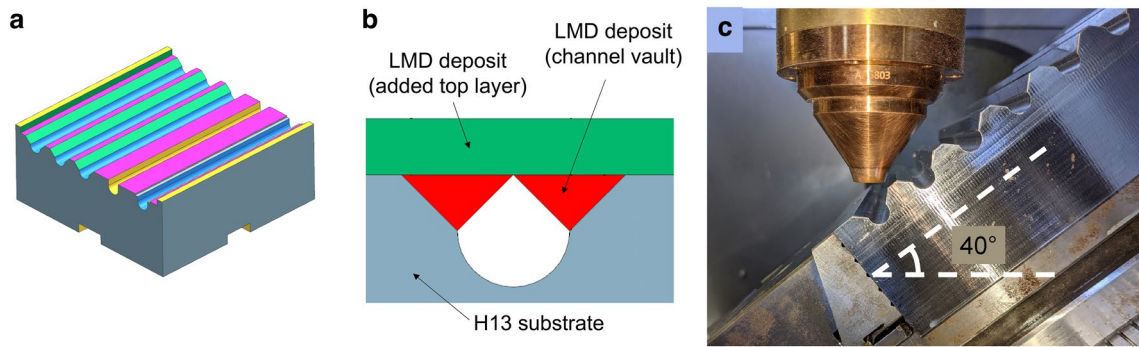


Fig. 6 a Machined demonstrator body, b hybrid LMD strategy for cooling channel creation, and c LMD fabrication of the cooling channel vaults

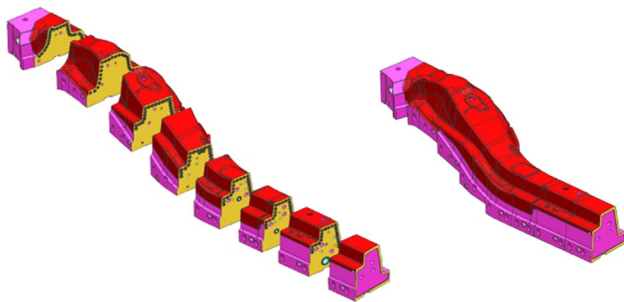


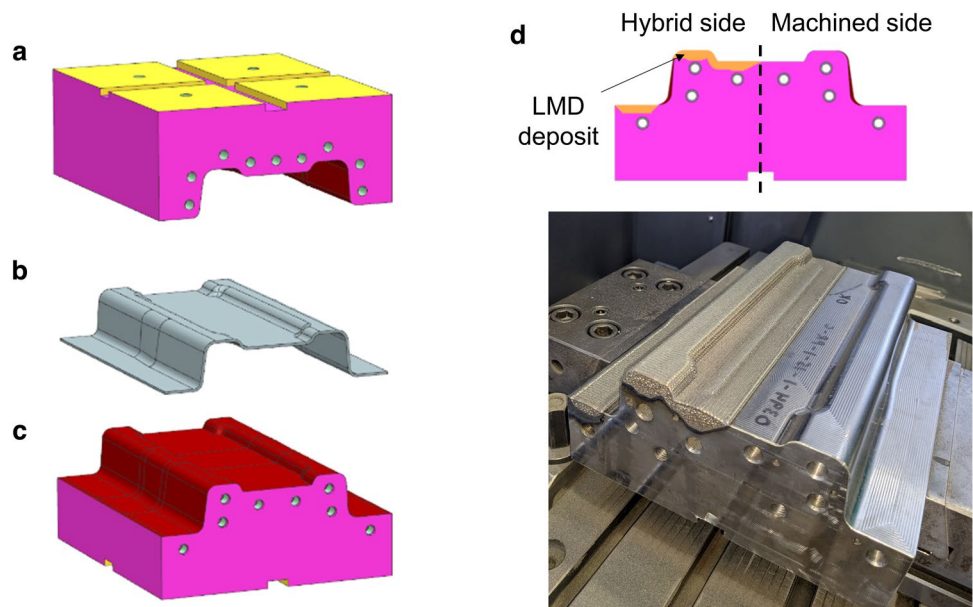
Fig. 7 Schematic of the assembly of hot stamping tool segments

blank made of heat-treated H13 hot work tool steel. A hybrid process was employed to fabricate the other side with the same geometry (Fig. 8d). Straight cooling channels were fabricated by drilling and a concave surface was generated by milling to allow the deposition of a Fe–Cr–Mo–V–Mn

steel cover by 5-axis LMD to achieve the designed tool geometry. An offset of 1 mm was maintained for the final surface finishing operation. The tool segment was not subjected to additional quenching and tempering treatment after the LMD process to avoid possible distortions between the two sides made of different materials. It should be emphasized that for this prototype only the top of the tool segment was produced by LMD, while the cooling channels were conventionally drilled to simplify the manufacturing of the segment. The purpose of this simplified tool design was to evaluate the effect of the Fe–Cr–Mo–V–Mn tool steel on the cooling efficiency of a hot stamping tool fabricated by the hybrid LMD process, compared to a tool conventionally machined from H13 hot work tool steel.

The upper die of the tool segment used for the stamping tests (Fig. 8a) was conventionally machined from a H13 hot work tool steel blank.

Fig. 8 Models of the a upper and c lower dies of the designed tool segment, b expected sheet geometry after hot stamping, and d view of the hybrid-manufactured tool segment before surface finishing



2.6 Testing of the hot stamping tool segment

Rockwell hardness testing (DIN 50157) was performed to compare the hardness of the two sides of the tool segment, using a portable DYNATEST SCX electronic hardness tester.

The service performance of the tool segment was validated in a hydraulic press to simulate its use in a real hot stamping process. Figure 9a shows the test setup, while the main parameters used in the stamping process are listed in Table 5. The press was equipped with four 50 kN load cells. The steel sheets to be stamped were heated in a furnace above the austenitization temperature before the forming operation and water was flowed into the cooling channels using a water manifold (Fig. 9b) during each pressing test. Four thermocouples (Fig. 9c) and a timing camera were used to measure the temperature peaks experienced by the

Table 5 Set of experimental parameters used for testing in the pilot plant

Parameter	Value
Blank thickness	2 mm
Press force	265 kN
Press speed	13 mm s ⁻¹
Average pressure during cooling stage	4.3 MPa
Furnace temperature	940 °C
Holding time in furnace	300 s
Cooling time	9 s

different zones of the tool segment during each stroke tryout. An aluminum foil was employed to protect the thermocouples from the heat radiated by the hot steel sheets. The temperature distribution in formed steel parts was qualitatively

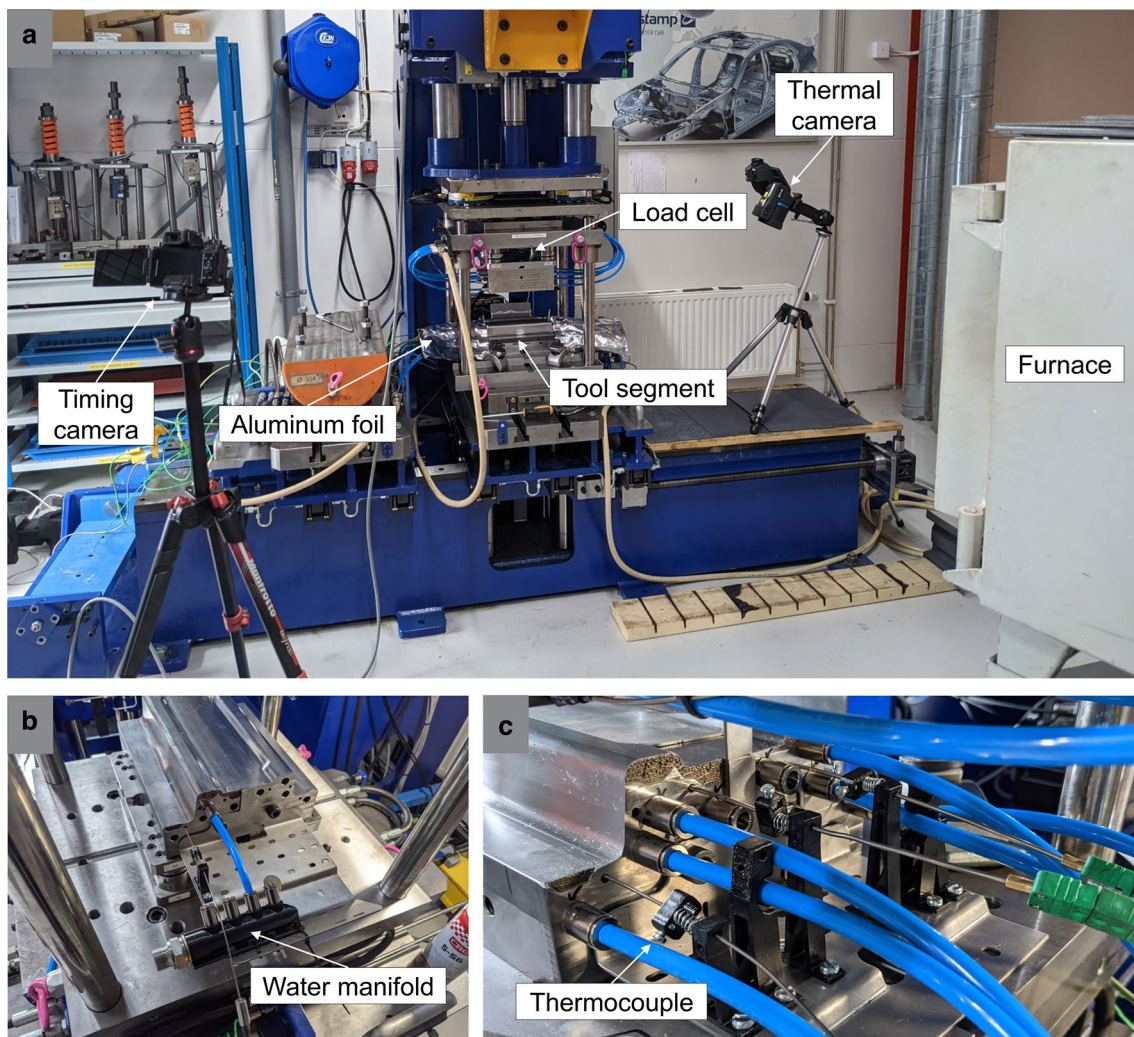


Fig. 9 Views of **a** the pilot plant used for the performance validation of the tool segment, **b** water manifold connected to the cooling channels, and **c** thermocouples connected to the tool segment

determined with a FLIR T1020 thermal camera immediately after the stamping operation. Since no specific calibration was performed, the absolute temperature values recorded by the thermal camera can be used for comparison purposes only, considering the different zones of each formed sheet and among different formed sheets.

The hardness of the hot stamped steel parts was measured using a Vickers hardness tester with the testing routine for HV_{10} (ISO 6507-1:2018).

3 Results and discussion

3.1 Density, microstructure, and hardness of LMD parts

The measured density of the as-built specimens and the theoretical density of the Fe–Cr–Mo–V–Mn alloy at 20 °C (estimated with ThermoCalc AB software based on actual composition) are provided in Table 6. Observation of the polished samples at low magnifications revealed equally spaced and aligned residual pores along the interface with the substrate and between the first two layers, as depicted in Fig. 10a. This inter-run porosity can be attributed to incomplete fusion of the feedstock material due to insufficient energy input or excessive material feeding provided during the deposition process [26, 27], as also confirmed by the presence of residual unmelted powder particles inside pores (Fig. 10b). Moreover, the presence

of significantly larger pores in the first few layers compared to the smaller pore size observed in the upper layers suggests that the low heat input of the process was further accentuated by a relatively high heat dissipation in close proximity to the cold substrate, which acted as a heat sink decreasing the amount of heat actually available for melting [28]. These defects tended to fade at upper positions of the deposit due to the higher temperature of the already deposited material which partially compensated for the low energy input.

The melt pool boundaries and scan tracks can be clearly observed in the optical micrographs of as-built specimens in the transverse (Fig. 11a) and top (Fig. 11b) cross sectional views, respectively.

The microstructure of the as-deposited material is shown in Fig. 12. A fine cellular structure exists at the boundary of the melt pools, while columnar dendrites are dominant in the inner regions, as highlighted in the higher magnification FE-SEM micrograph of Fig. 12b. These cell morphologies resulted from the different solidification conditions experienced by the different regions of the melt pool. The border of the melt pool experienced a higher thermal gradient during solidification due to the direct contact with the already solidified material at relatively low temperature. According to solidification maps [29], high thermal gradients in combination with rapid cooling rates during LMD lead to a fine cellular microstructure that is consistently observed at the melt pool boundaries. On the other hand, the inner region of the melt pool is subjected to a lower temperature gradient, resulting in the preferential growth of columnar dendrites. It can be observed that the dendrites are mostly oriented perpendicularly to the melt pool boundary, indicating that preferential growth occurred in the direction opposite to the heat flow towards the already solidified material. Finally, it is assumed that martensite and retained austenite are the main

Table 6 Density of as-built LMD parts

Measured density	Theoretical density	Relative density
$7.55 \pm 0.15 \text{ g cm}^{-3}$	7.78 g cm^{-3}	97%

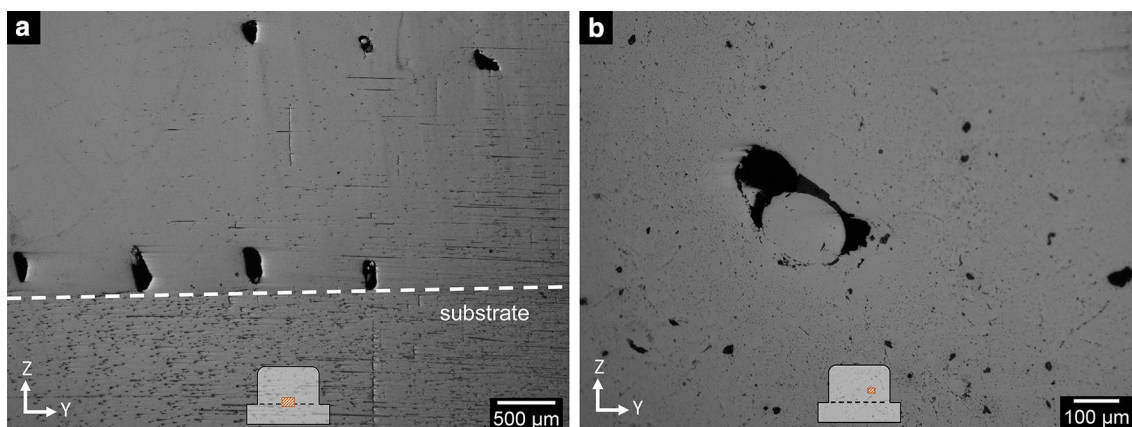


Fig. 10 **a** Interlayer porosity and **b** lack of fusion defect found in as-built LMD specimens. The schematic drawings indicate the area of the sample where the micrographs were collected

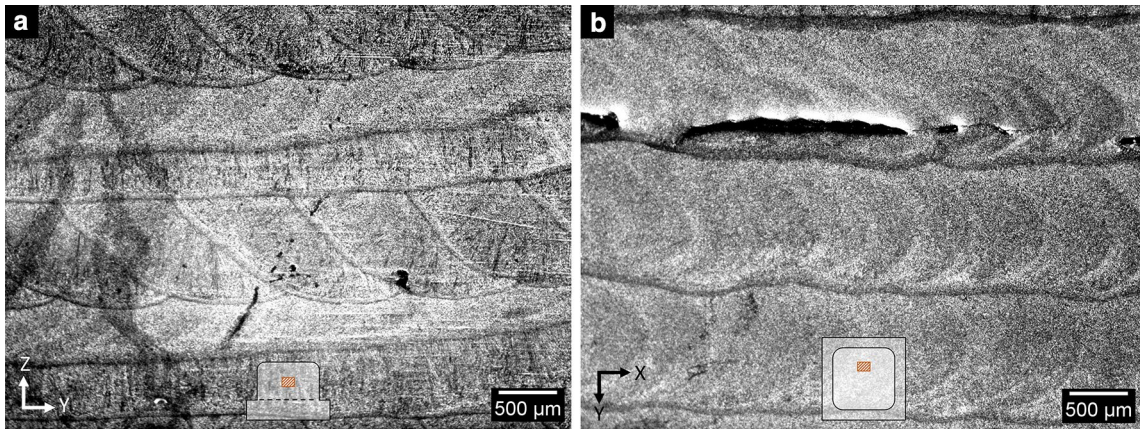


Fig. 11 **a** Melt pool boundaries and **b** scan tracks observed in as-built LMD specimens. The schematic drawings indicate the area of the sample where the micrographs were collected

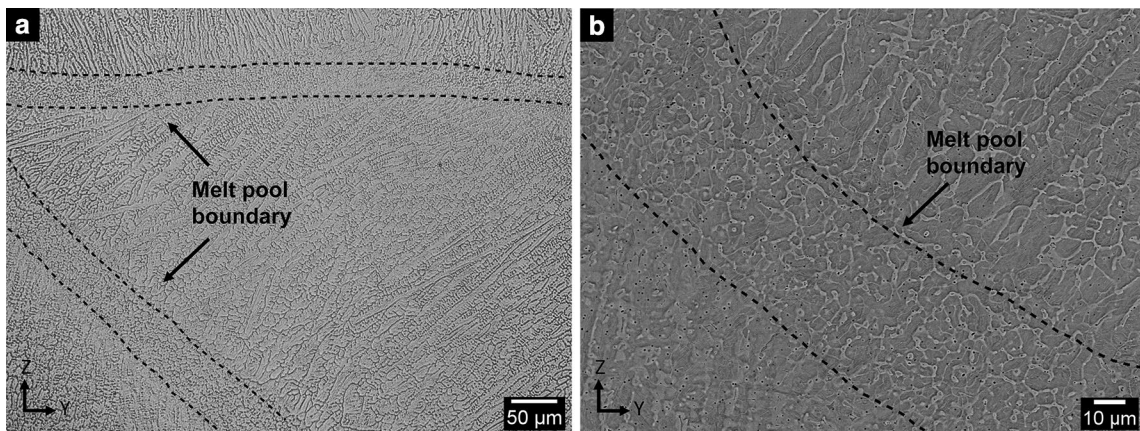


Fig. 12 **a** Optical and **b** FE-SEM micrographs depicting the LMD as-built microstructure of the Fe–Cr–Mo–V–Mn alloy

constituents of the as-built microstructure (Fig. 12b), similarly to what was observed by Chen et al. [30] in as-printed H13 hot work tool steel specimens fabricated by LMD.

The dendritic structure vanished during the austenitizing step, and a tempered martensitic microstructure was generated after the application of the conventional quenching and tempering treatment, as shown in Fig. 13. In addition, a homogeneous microstructure was observed along the whole cross-section of the specimens. Therefore, the developed material microstructure responds to standard quenching and tempering treatment similarly to H13 hot work tool steel, with the formation of fine constituents mainly consisting of tempered martensite [31]. The precipitation of Mo_2C , V_6C_5 , and M_{23}C_6 ($\text{M}=\text{Cr}, \text{Fe}, \text{Mo}$) carbides was also predicted by ThermoCalc simulations, but could not be precisely verified by SEM in this investigation.

Figure 14 shows a representative longitudinal cross section of an as-built sample and the corresponding hardness profile measured along the indicated vertical line. The deposit displayed a uniform hardness along its height, averaging around $600 \text{ HV}_{0.3}$. The higher hardness compared to LMD processed H13 hot work tool steel ($\sim 540 \text{ HV}_{0.3}$ [30]) can be attributed to the higher content of carbide-former alloying elements. This increase in hardness is beneficial because it can result in increased resistance against wear and thermal fatigue [32], thus potentially prolonging the service life of hybrid-manufactured hot stamping tools. The first two deposited layers showed a slightly lower hardness (543 and $557 \text{ HV}_{0.3}$, respectively) compared to the upper layers, presumably due to the dilution of the Fe–Cr–Mo–V–Mn alloy with the 316L stainless steel substrate ($\sim 180 \text{ HV}_{0.3}$ hardness).

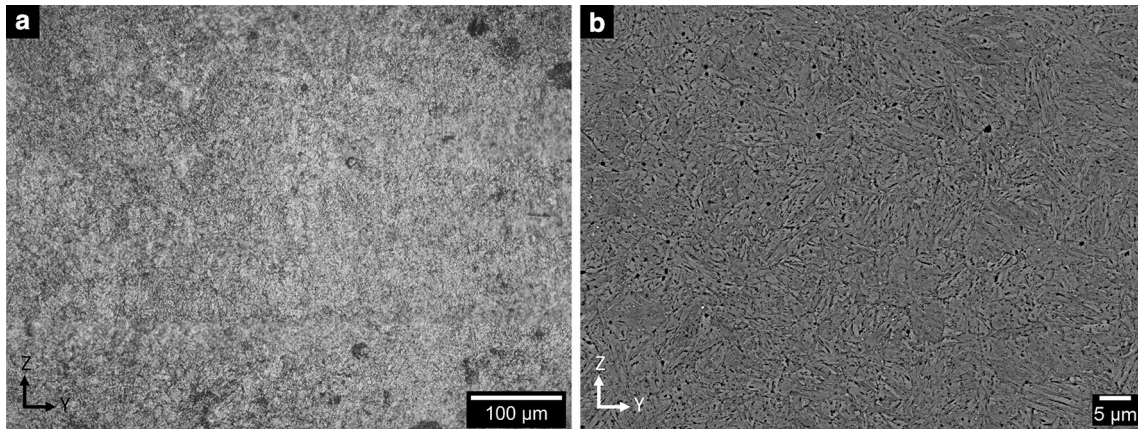


Fig. 13 **a** Optical and **b** FE-SEM micrographs showing the microstructure of heat-treated LMD specimens

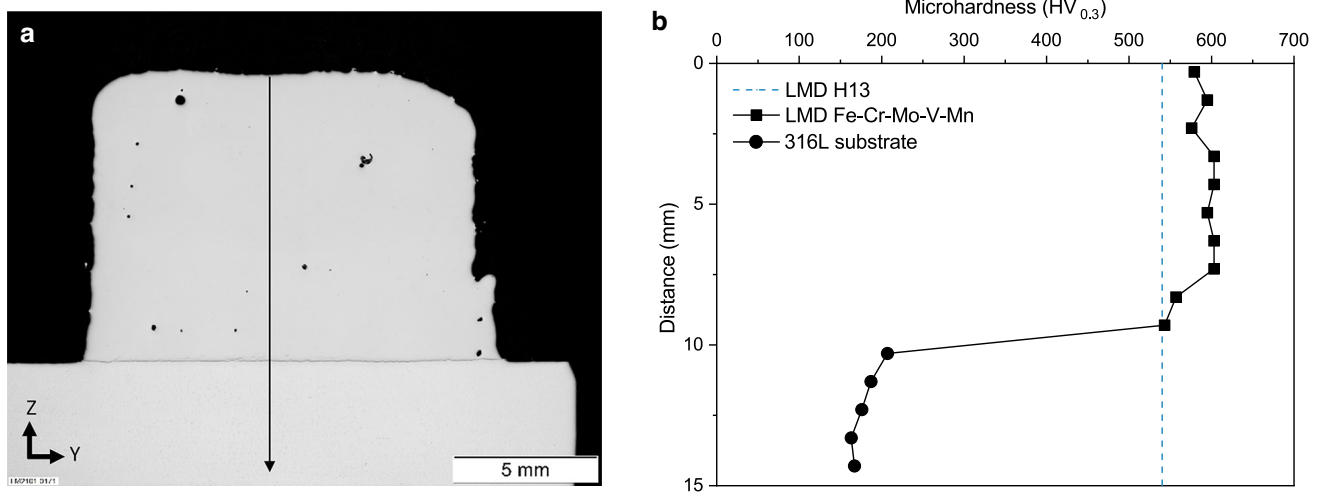


Fig. 14 **a** Cross-section of an as-built LMD specimen with indication of the measurement line and **b** measured hardness profile compared to the hardness of LMD processed H13 hot work tool steel [30]

3.2 Thermophysical properties of LMD parts

Figure 15 shows the dilatation curve and the calculated coefficient of thermal expansion (CTE) of the investigated steel in as-built and heat-treated conditions. The non-linearity observed at around 500 °C during heating of the as-built material can be attributed to the decomposition of retained austenite, which is thermodynamically unstable. Despite the relatively high transformation temperatures predicted for the Fe–Cr–Mo–V–Mn alloy, retained austenite may have remained at the end of the deposition process because the high cooling rate of LMD hinders carbide precipitation and growth [30]. As a result, a higher amount of

alloying elements remains in solid solution in the austenite phase, thus reducing the real martensite start temperature of the material [30]. No evidence of the martensitic transformation taking place during cooling can be observed in the diagram of Fig. 15b, indicating that full decomposition of the retained austenite occurred during the heating stage. The heat-treated material exhibits a more stable behavior because the retained austenite was fully transformed into martensite during the tempering treatment.

The linear CTE was calculated as the first derivative of the dilatation curve with respect to the temperature in the heating portion (Fig. 15a), using steps of 25 °C according to the following equation [33]:

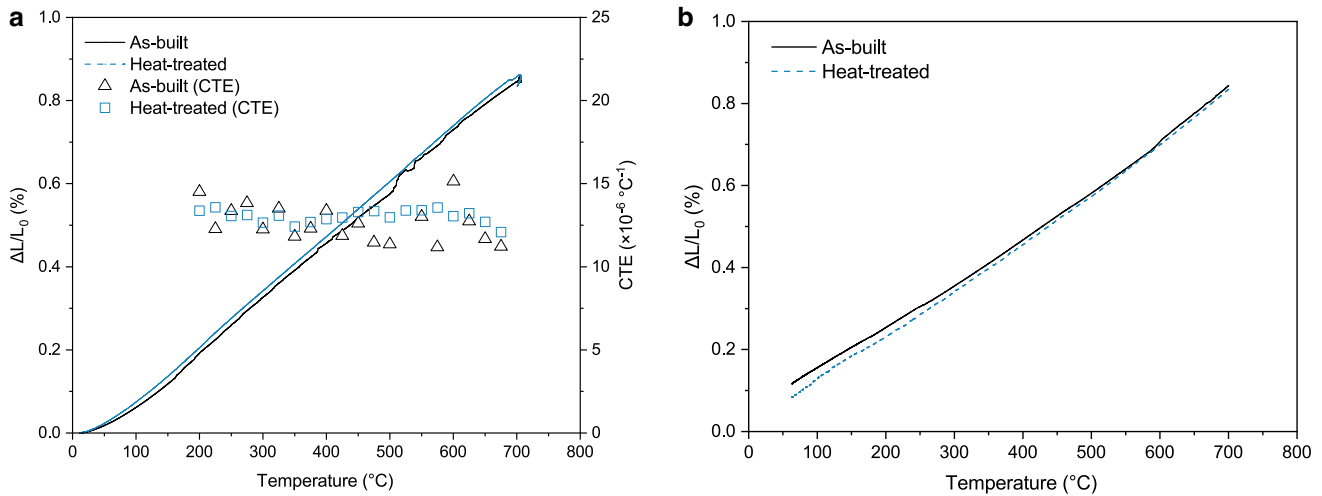


Fig. 15 Dilatation curve and CTE trend of as-built and heat-treated LMD specimens recorded during **a** heating and **b** cooling

$$\alpha = \frac{1}{L_1} \frac{L_2 - L_1}{T_2 - T_1}$$

where $L_2 - L_1$ is the change of specimen length due to temperature variation from T_1 to T_2 . The average CTE calculated in the temperature range between 200 and 700 °C, where the dilatation curves are about linear, is $12.50 \pm 1.16 \times 10^{-6} \text{ }^\circ\text{C}^{-1}$ for the as-built material and $12.85 \pm 0.91 \times 10^{-6} \text{ }^\circ\text{C}^{-1}$ for the heat-treated material. These values are comparable with the CTE of H13 hot work tool steel ($12.6 \times 10^{-6} \text{ }^\circ\text{C}^{-1}$ [34]), indicating that the Fe–Cr–Mo–V–Mn alloy is suitable to be directly deposited via LMD on a H13 hot work tool steel substrate. Indeed, when joining dissimilar metallic materials by AM, low discrepancy in their CTE is crucial to avoid large thermal stresses that may induce defects such as cracking and delamination at the interface [35]. In addition, a large mismatch in the CTE of different regions of the tool would cause fluctuating strains to develop as a result of the heating and cooling cycles during the hot stamping process, making it more susceptible to thermal fatigue failure. The CTE values calculated for temperatures lower than 200 °C were not reported because the quality of the collected data was affected by the thermal transient due to the inertia of the materials under the relatively high heating rate used for the experiments ($10 \text{ }^\circ\text{C min}^{-1}$).

Figure 16 shows the thermal diffusivity data of as-built specimens collected during LFA experiments. The error bars on both thermal diffusivity and temperature values are reported in the graph. The uncertainty on the thermal diffusivity values can be primarily attributed to the different amount and distribution of residual porosity in the tested specimens, while the deviation on the temperature values is due to the allowance of $\pm 7 \text{ }^\circ\text{C}$ set for the measurements. The temperature dependence is the same as reported by Džugan et al. [36] for

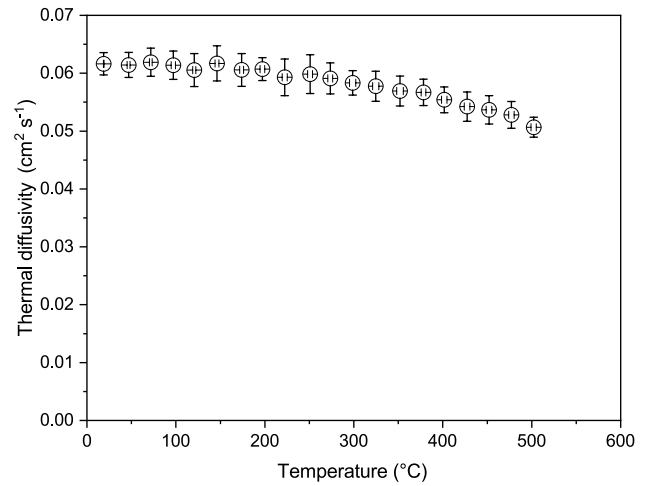


Fig. 16 Thermal diffusivity of as-built parts as a function of temperature

LPBF processed H13 hot work tool steel. The average thermal diffusivity at room temperature is $6.16 \pm 0.19 \text{ mm}^2 \text{ s}^{-1}$, which is in line with the values reported by Arrizubieta et al. [37] for laser-deposited H13 hot work tool steel. This value is comparable, although slightly lower, than the thermal diffusivity of wrought H13 hot work tool steel ($6.86 \text{ mm}^2 \text{ s}^{-1}$), calculated from the data found in the literature [38–40] using the following equation [37]:

$$\alpha = \frac{k}{\rho \times c_p}$$

where α is the thermal diffusivity, k is the thermal conductivity, ρ is the density, and c_p is the specific heat of the material. Since thermal diffusivity is proportional to thermal

conductivity, this is a further indication that the proposed alloy is a good candidate for the direct deposition on a H13 hot work tool steel substrate. Indeed, the difference in thermal conductivity is a key factor to be considered when joining dissimilar metallic materials, as a large mismatch would induce a non-uniform cooling of the bimetallic structure during the deposition process. Under this condition, the material with higher thermal conductivity would experience a faster cooling, but its contraction would be constrained by the counterpart, generating thermal stresses that may promote crack formation [38]. On the contrary, a similar thermal conductivity between the two materials ensures a more uniform temperature variation in the tool during the heating and cooling cycles of hot stamping operations, thus attenuating the detrimental effects of thermal fatigue. The slight reduction in

thermal diffusivity of the Fe–Cr–Mo–V–Mn alloy compared to H13 hot work tool steel can be primarily attributed to the residual porosity [41, 42] and to the small size of the columnar dendrites observed in the as-built specimens (Fig. 12), resulting in a large amount of interfaces that decrease the mean free path of electrons and, consequently, the electronic contribution to heat conduction when compared to the wrought steel microstructure [37]. The reduction can additionally be attributed to the larger content of alloying elements (such as chromium, molybdenum, and manganese) in the investigated material as compared to standard H13 hot work tool steel. These alloying elements decrease the thermal conductivity of steels [43, 44] because they introduce lattice distortions and, consequently, hinder thermal energy transport by lattice waves [45].

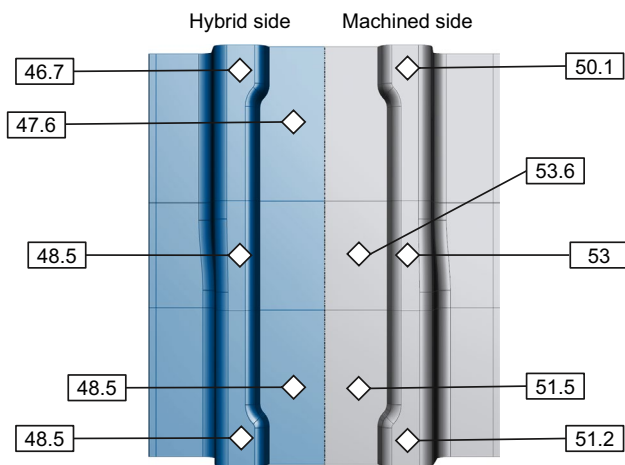


Fig. 17 HRC hardness distribution measured on the surface of the heat-treated machined side and the untreated hybrid-manufactured side of the tool segment

3.3 Pilot plant testing

Figure 17 shows a map of the Rockwell hardness values measured on the surface of the manufactured tool segment. The hybrid-manufactured side of the tool segment displayed a slightly lower hardness than the conventionally machined side, as it was not subjected to a specific quenching and tempering treatment. However, this gap is supposed to be reduced or eliminated in a real hybrid-manufactured component once the heat treatment is performed on the whole tool to meet the technical requirements for hot stamping tools (> 50 HRC hardness [5]). The hardness of the tool segment prototype was still considered sufficiently high to withstand the short-term service conditions for the testing in the pilot plant.

Figure 18a displays the regions of the tool segment where the temperature profiles shown in Fig. 18b were recorded during the pilot plant testing. Each temperature peak

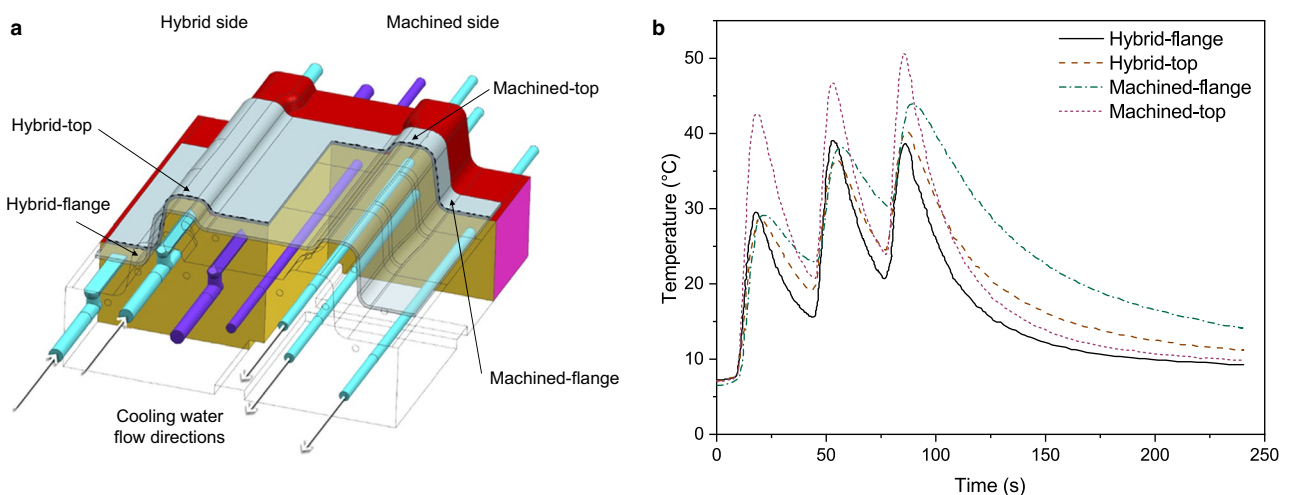


Fig. 18 **a** Measurement zones and **b** thermal profiles recorded at the hybrid-manufactured and machined side of the hot stamping tool segment during testing in the pilot plant

corresponds to one press stroke tryout, i.e., one steel blank being formed and quenched. The hybrid-manufactured side experienced lower temperature peaks compared to the conventionally machined side, due to less efficient heat extraction from the hot blanks by the LMD deposited material, having a slightly lower thermal conductivity than H13 hot work tool steel. Therefore, the portion of the steel blank that was formed by the hybrid-manufactured side of the tool segment in each hot stamping cycle was subjected to a lower cooling rate and experienced a slightly higher temperature profile when removed from the die compared to the region formed by the machined side of the tool (Fig. 19a). As a result, the steel sheets showed a lower hardness in the region that was formed by the hybrid-manufactured side of the tool segment in each press stroke tryout (Fig. 19c).

As the number of hot stamping cycles carried out increased, the hardness of the formed parts decreased (Fig. 19c) due to the lower cooling rate induced by the tool segment still being relatively hot from the previous cycle. The qualitative thermal images in Fig. 19a, b show that the part formed in the sixth pressing test featured an overall higher temperature when removed from the die compared to the part formed in the third run. The blank portion that was formed by the machined side of the tool segment experienced only a slight reduction in hardness when performing more than three hot stamping cycles. On the other hand, the hardness of the portion formed by the hybrid-manufactured side decreased appreciably already from the second

cycle, due to slower cooling of the LMD deposit made of Fe–Cr–Mo–V–Mn material with lower thermal conductivity.

Although the hybrid-manufactured side of the tool segment exhibited a lower thermal performance than the machined counterpart, it should be remarked that the tool segment was not heat treated after the LMD process to avoid distortions between the two dissimilar sides. This may have negatively affected the thermal performance of the LMD deposit, as tempering treatment is recognized to improve the thermal conductivity of tool steels by carbide precipitation, which reduces lattice distortion [46]. Moreover, the potential of conformal profiles for the hybrid-manufactured cooling channels in increasing the efficiency of the cooling system has not yet been exploited in this version of the prototype. It is expected that a higher cooling efficiency will be achieved after implementing specifically designed channels in the tool segments, taking advantage of the opportunities offered by LMD manufacturing.

4 Conclusions

Based on the experimental results, the main conclusions of this investigation can be recapped as follows.

- (1) Microstructural observations of the LMD specimens showed that, after being heat treated, the Fe–Cr–

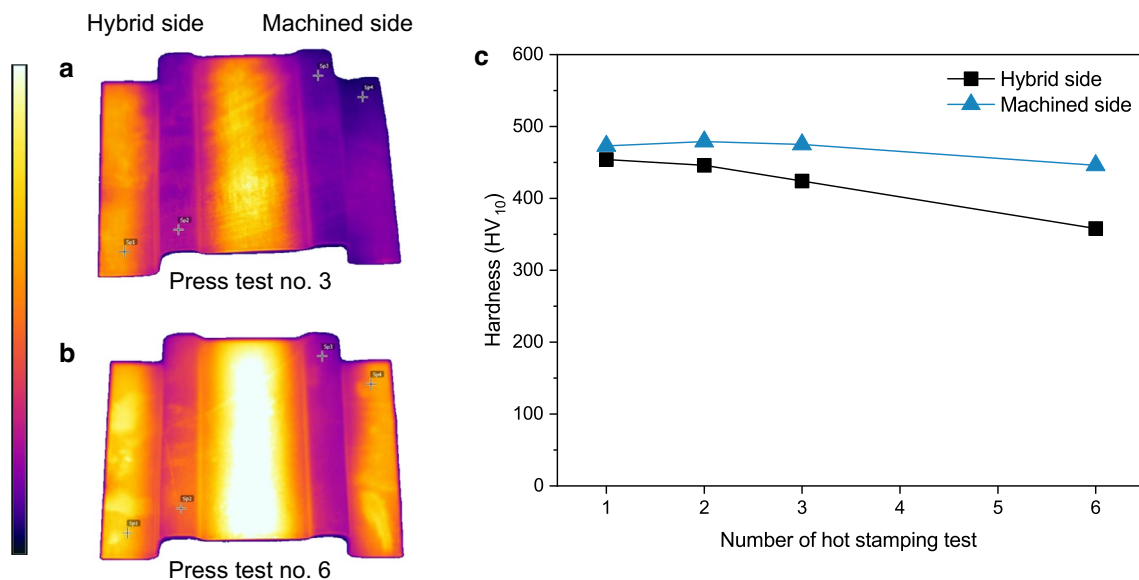


Fig. 19 Thermal maps of formed parts immediately after hot stamping tests **a** number 3 and **b** number 6, and **c** hardness measured in the regions of steel parts formed with the hybrid-manufactured and the

machined side of the tool segment, respectively, as a function of the number of hot stamping cycles performed

Mo–V–Mn alloy develops a fine tempered martensitic structure similar to that observed in a quenched and tempered H13 hot work tool steel. In addition, the material exhibited expansion behavior and thermal diffusivity comparable to those of H13 hot work tool steel. The similarity in thermophysical properties promotes the developed alloy to be a promising candidate for the direct deposition on a tool steel body for the fabrication of conformal cooling channels, while mitigating thermal fatigue issues caused by the heating and cooling cycles of the hot stamping process.

- (2) The as-deposited material exhibited a slight increase in hardness compared to LMD processed H13 hot work tool steel. This can potentially enhance the wear and thermal fatigue resistance of hot stamping tools fabricated by hybrid LMD employing the Fe–Cr–Mo–V–Mn steel compared to hybrid tools made by H13 hot work tool steel, resulting in longer tool service life.
- (3) A hybrid manufacturing process integrating conventional machining and 5-axis LMD was successfully employed to fabricate bimetallic cooling channels by directly depositing the Fe–Cr–Mo–V–Mn material on a machined H13 hot work tool steel substrate. No intermediate material needed to be placed to improve the compatibility between the machined substrate and the additively manufactured sections of the component, which reduced the complexity of the manufacturing process compared to previous studies reported in the literature.
- (4) The hybrid-manufactured tool segment tested in the pilot plant exhibited a lower thermal performance than the homogeneous machined counterpart owing to the slightly lower thermal conductivity of the Fe–Cr–Mo–V–Mn material compared to H13 hot work tool steel. However, the cooling efficiency of the hybrid LMD-processed part can be further enhanced by applying a proper quenching and tempering heat treatment to increase the thermal conductivity of the Fe–Cr–Mo–V–Mn deposited layers and by implementing more efficient conformal cooling channels, thus taking full advantage of the design flexibility offered by additive manufacturing.

An improved version of the prototype, featuring an optimized network of conformal cooling channels and the final heat-treated condition, will be designed and assessed in a future study. A modified heat treatment procedure could also be developed taking into account the different chemical composition of the proposed alloy and the peculiar microstructure resulting from the LMD process.

Acknowledgements The investigations were carried out within the frame of SPACEMAN project funded by EIT-Raw Materials in 2018–2021. The Italian Ministry of Education, University and Research is acknowledged for the support provided through the project "Department of Excellence LIS4.0—Lightweight and Smart Structures for Industry 4.0".

Author contributions TR: investigation, data curation, formal analysis, writing—original draft, and writing—review and editing. MA: investigation, methodology, and writing—review and editing. SB: investigation and resources. FB: investigation, writing—original draft, and data curation. RC: project administration, supervision, validation, and writing—review and editing. HG: investigation, methodology, resources, and data curation. EL: conceptualization, funding acquisition, project administration, resources, and supervision. PU: investigation, methodology, resources, and data curation. CW: conceptualization and investigation. MV: conceptualization, funding acquisition, project administration, supervision, and writing—review and editing.

Funding Open access funding provided by Politecnico di Milano within the CRUI-CARE Agreement. European Institute of Innovation and Technology (Grant no. 17070).

Data availability The data that support the findings of this study are available from the corresponding author upon reasonable request.

Declarations

Conflict of interest The authors declare that they have no conflict of interest.

Open Access This article is licensed under a Creative Commons Attribution 4.0 International License, which permits use, sharing, adaptation, distribution and reproduction in any medium or format, as long as you give appropriate credit to the original author(s) and the source, provide a link to the Creative Commons licence, and indicate if changes were made. The images or other third party material in this article are included in the article's Creative Commons licence, unless indicated otherwise in a credit line to the material. If material is not included in the article's Creative Commons licence and your intended use is not permitted by statutory regulation or exceeds the permitted use, you will need to obtain permission directly from the copyright holder. To view a copy of this licence, visit <http://creativecommons.org/licenses/by/4.0/>.

References

1. Muvunzi R, Dimitrov DM, Matope S, Harms T (2021) A case study on the design of a hot stamping tool with conformal cooling channels. *Int J Adv Manuf Technol* 114:1833–1846. <https://doi.org/10.1007/s00170-021-06973-z>
2. Reimer L, Kaluza A, Cerdas F, Meschke J, Vietor T, Herrmann C (2020) Design of eco-efficient body parts for electric vehicles considering life cycle environmental information. *Sustain* 12:5838. <https://doi.org/10.3390/su12145838>
3. Czerwinski F (2021) Current trends in automotive lightweighting strategies and materials. *Materials* 14:6631. <https://doi.org/10.3390/ma14216631>
4. Arrizubieta JI, Cortina M, Ostolaza M, Ruiz JE, Lamikiz A (2019) Case Study: modeling of the cycle time reduction in a B-Pillar hot stamping operation using conformal cooling. *Procedia Manuf* 41:50–57. <https://doi.org/10.1016/j.promfg.2019.07.028>

5. Chantzis D, Liu X, Politis DJ, El Fakir O, Chua TY, Shi Z, Wang L (2020) Review on additive manufacturing of tooling for hot stamping. *Int J Adv Manuf Technol* 109:87–107. <https://doi.org/10.1007/s00170-020-05622-1>
6. Lim W, Choi H, Ahn S, Kim B (2014) Cooling channel design of hot stamping tools for uniform high-strength components in hot stamping process. *Int J Adv Manuf Technol* 70:1189–1203. <https://doi.org/10.1007/s00170-013-5331-0>
7. Feng S, Kamat AM, Pei Y (2021) Design and fabrication of conformal cooling channels in molds: review and progress updates. *Int J Heat Mass Transf* 171:121082. <https://doi.org/10.1016/j.jhema.2021.121082>
8. Dang XP, Park HS (2011) Design of u-shape milled groove conformal cooling channels for plastic injection mold. *Int J Precis Eng Manuf* 12:73–84. <https://doi.org/10.1007/s12541-011-0009-8>
9. Rahim SZA, Sharif S, Zain AM, Nasir SM, Mohd Saad R (2016) Improving the quality and productivity of molded parts with a new design of conformal cooling channels for the injection molding process. *Adv Polym Technol* 35:1–10. <https://doi.org/10.1002/adv.21524>
10. Tan C, Wang D, Ma W, Chen Y, Chen S, Yang Y, Zhou K (2020) Design and additive manufacturing of novel conformal cooling molds. *Mater Des* 196:109147. <https://doi.org/10.1016/j.matdes.2020.109147>
11. Hölker R, Haase M, Ben Khalifa N, Tekkaya AE (2015) Hot extrusion dies with conformal cooling channels produced by additive manufacturing. *Mater Today: Proc* 2:4838–4846. <https://doi.org/10.1016/j.matpr.2015.10.028>
12. Phull GS, Kumar S, Walia RS (2018) Conformal cooling for molds produced by additive manufacturing: a review. *Int J Mech Eng Technol* 9:1162–1172
13. Shinde MS, Ashtankar KM (2017) Additive manufacturing-assisted conformal cooling channels in mold manufacturing processes. *Adv Mech Eng* 9:1–14. <https://doi.org/10.1177/1687814017699764>
14. Asnafi N, Rajalampi J, Aspenberg D, Alveflo A (2020) Production tools made by additive manufacturing through laser-based powder bed fusion. *BHM Berg-Huettenmaenn Monatsh* 165:125–136. <https://doi.org/10.1007/s00501-020-00961-8>
15. Muvunzi R, Matope S, Madyibi X, Swart CB, Nagel M (2020) Industry case study: process chain for manufacturing of a large hybrid hot stamping tool with conformal cooling channels. *Int J Adv Manuf Technol* 110:1723–1730. <https://doi.org/10.1007/s00170-020-05992-6>
16. Terrazas CA, Gaytan SM, Rodriguez E, Espalin D, Murr LE, Medina F, Wicker RB (2014) Multi-material metallic structure fabrication using electron beam melting. *Int J Adv Manuf Technol* 71:33–45. <https://doi.org/10.1007/s00170-013-5449-0>
17. Liu C, Cai Z, Dai Y, Huang N, Xu F, Lao C (2018) Experimental comparison of the flow rate and cooling performance of internal cooling channels fabricated via selective laser melting and conventional drilling process. *Int J Adv Manuf Technol* 96:2757–2767. <https://doi.org/10.1007/s00170-018-1799-y>
18. Gibson I, Rosen D, Stucker B, Khorasani M (2021) Directed energy deposition. In: *Addit manuf technol*, pp 285–286. <https://doi.org/10.1007/978-3-030-56127-7>
19. Cortina M, Arrizubieta JI, Calleja A, Ukar E, Alberdi A (2018) Case study to illustrate the potential of conformal cooling channels for hot stamping dies manufactured using hybrid process of laser metal deposition (LMD) and milling. *Met* 8:102. <https://doi.org/10.3390/MET8020102>
20. Hong MP, Kim JJ, Kim WS, Lee MK, Bae KM, Kim YS, Sung JH (2020) Heterogeneous material additive manufacturing for hot-stamping die. *Metals* 10:1210. <https://doi.org/10.3390/MET10091210>
21. Shinde MS, Ashtankar KM, Kuthe AM, Dahake SW, Mawale MB (2018) Direct rapid manufacturing of molds with conformal cooling channels. *Rapid Prototyp J* 24:1347–1364. <https://doi.org/10.1108/RPJ-12-2016-0199>
22. H13 Tool Steel | 1.2344 | SKD61 Hot Work Steel - Otai Special Steel. <https://www.astmsteel.com/product/h13-tool-steel-x40crmov5-1-skd61-hot-work-steel/>. Accessed 10 Mar 2022
23. Mesquita RA, Schneider R, Gonçalves CS (2018) Heat treating of hot-work tool steels. *Heat Treat Irons Steels* 4:336–346. <https://doi.org/10.31399/asm.hb.v04d.a0005974>
24. Akhtar SS, Arif AFM, Yilbas BS (2017) Gas nitriding of h13 tool steel used for extrusion dies: numerical and experimental Investigation. *Compr Mater Finish*. <https://doi.org/10.1016/B978-0-12-803581-8.09174-8>
25. Brandt SD, Schön CG (2017) A thermodynamic study of a constitutional diagram for duplex stainless steels. *J Phase Equilibria Diffus* 38:268–275. <https://doi.org/10.1007/s11669-017-0537-8>
26. Dass A, Moridi A (2019) State of the art in directed energy deposition: from additive manufacturing to materials design. *Coatings* 9:1–26. <https://doi.org/10.3390/COATINGS9070418>
27. Dalae M, Cerrutti E, Dey I, Leinenbach C, Wegener K (2022) Parameters development for optimum deposition rate in laser DMD of stainless steel EN X3CrNiMo13–4. *Lasers Manuf Mater Process* 9:17. <https://doi.org/10.1007/s40516-021-00161-3>
28. Zhao X, Lv Y, Dong S, Yan S, He P, Liu X, Liu Y (2020) The effect of thermal cycling on direct laser-deposited gradient H13 tool steel: microstructure evolution, nanoprecipitation behaviour, and mechanical properties. *Mater Today Commun* 25:101390. <https://doi.org/10.1016/j.mtcomm.2020.101390>
29. Kou S (2003) Basic solidification concepts. In: *Weld Metall*, pp 165–166
30. Chen C, Yan K, Qin L, Zhang M, Wang X, Zou T, Hu Z (2017) Effect of heat treatment on microstructure and mechanical properties of laser additively manufactured AISI H13 tool steel. *J Mater Eng Perform* 26:5577–5589. <https://doi.org/10.1007/s11665-017-2992-0>
31. Mutlu I, Oktay E, Ekinici S (2013) Characterization of microstructure of H13 tool steel using ultrasonic measurements. *Russ J Nondestruct Test* 49:112–120. <https://doi.org/10.1134/S106183091302006X>
32. Mellouli D, Haddar N, Köster A, Ferid H (2014) Hardness effect on thermal fatigue damage of hot-working tool steel. *Eng Fail Anal* 45:85–95. <https://doi.org/10.1016/j.engfailanal.2014.06.007>
33. Romano T, Migliori E, Mariani M, Lecis N, Vedani M (2022) Densification behaviour of pure copper processed through cold pressing and binder jetting under different atmospheres. *Rapid Prototyp J*. <https://doi.org/10.1108/RPJ-09-2021-0243>
34. Saifullah ABM, Masood SH, Nikzad M (2016) An investigation on fabrication of conformal cooling channel with direct metal deposition for injection moulding. In: *Reference module in materials science and materials engineering*. <https://doi.org/10.1016/B978-0-12-803581-8.04023-6>
35. Nam S, Cho H, Kim C, Kim YM (2018) Effect of process parameters on deposition properties of functionally graded STS 316/Fe manufactured by laser direct metal deposition. *Metals* 8:607. <https://doi.org/10.3390/met8080607>
36. Džugan J, Halmešová K, Ackermann M, Koukolíková M, Trojanová Z (2020) Thermochemical acta thermo-physical properties investigation in relation to deposition orientation for SLM deposited H13 steel. *Thermochim Acta* 683:178479. <https://doi.org/10.1016/j.tca.2019.178479>
37. Arrizubieta JI, Cortina M, Mendioroz A, Salazar A, Lamikiz A (2020) Thermal diffusivity measurement of laser-deposited AISI H13 tool steel and impact on cooling performance of hot stamping tools. *Metals* 10:154. <https://doi.org/10.3390/met10010154>

38. Zhang X, Sun C, Pan T, Flood A, Zhang Y, Li L, Liou F (2020) Additive manufacturing of copper—H13 tool steel bi-metallic structures via Ni-based multi-interlayer. *Addit Manuf* 36:101474. <https://doi.org/10.1016/j.addma.2020.101474>
39. Kurzynowski T, Stopyra W, Gruber K, Ziółkowski G, Kuznicka B, Chlebus E (2019) Effect of scanning and support strategies on relative density of SLM-ed H13 steel in relation to specimen size. *Materials* 12:239. <https://doi.org/10.3390/ma12020239>
40. Pinkerton AJ, Li L (2005) Direct additive laser manufacturing using gas- and water-atomised H13 tool steel. *Int J Adv Manuf Technol* 25:471–479. <https://doi.org/10.1007/s00170-003-1844-2>
41. Francl J, Kingery WD (1954) Thermal conductivity: IX, experimental investigation of effect of porosity on thermal conductivity. *J Am Ceram Soc* 37:99–107. <https://doi.org/10.1111/j.1551-2916.1954.tb20108.x>
42. Yegyan Kumar A, Wang J, Bai Y, Huxtable ST, Williams CB (2019) Impacts of process-induced porosity on material properties of copper made by binder jetting additive manufacturing. *Mater Des* 182:108001. <https://doi.org/10.1016/j.matdes.2019.108001>
43. Wang G, Li Y (2019) Effects of alloying elements and temperature on thermal conductivity of ferrite. *J Appl Phys* 126:125118. <https://doi.org/10.1063/1.5115441>
44. Terada Y, Ohkubo K, Mohri T, Suzuki T (2002) Effects of alloying additions on thermal conductivity of ferritic iron. *ISIJ Int* 42:322–324. <https://doi.org/10.2355/isijinternational.42.322>
45. Chu TK, Ho CY (1978) Thermal conductivity and electrical resistivity of eight selected AISI stainless steels. *Therm Conduct* 15:79–104. https://doi.org/10.1007/978-1-4615-9083-5_12
46. Wilzer J, Weber S, Escher C, Theisen W (2012) On the relationship of heat treatment, microstructure, mechanical properties, and thermal conductivity of tool steels. In: 9th Int Tool Conference, pp 143–152

Publisher's Note Springer Nature remains neutral with regard to jurisdictional claims in published maps and institutional affiliations.